BJPS

Brazilian Journal of Pharmaceutical Sciences

DOI: http://dx.doi.org/10.1590/s2175-97902025e24545

Article

Synthesis and activity evaluation of new second-generation santacruzamate a analogs against breast cancer cells

Túlio Resende Freitas[1*], Samira Fagundes de Andrade[2], Fernanda Cristina Gontijo Evangelista[3], Silmara Nunes Andrade[1], Caique Lopes Duarte[1], Hélio Batista dos Santos[4], Ralph Gruppi Thomé[4], Jorge Luiz Humberto[2], Rossimiriam Pereira de Freitas[5], Adriano de Paula Sabino[3], Flaviane Francisco Hilário[2*], Fernando de Pilla Varotti[1*]

[1]Núcleo de Pesquisa em Química Biológica (NQBio), Universidade Federal de São João del-Rei, Campus Centro Oeste, Divinópolis, MG, Brazil, [2]Departamento de Química (DEQUI), Instituto de Ciências Exatas e Biológicas (ICEB), Universidade Federal de Ouro Preto, Campus Universitário Morro do Cruzeiro, Ouro Preto, MG, Brazil, [3]Departamento de Análises Clínicas e Toxicológicas, Faculdade de Farmácia, Universidade Federal de Minas Gerais, Campus Pampulha, Belo Horizonte, MG, Brazil, [4]Laboratório de Processamento de Tecido, Universidade Federal de São João del-Rei, Campus Centro Oeste, Divinópolis, MG, Brazil, [5]Departamento de Química, Instituto de Ciências Exatas, Universidade Federal de Minas Gerais, Campus Pampulha, Belo Horizonte, MG, Brazil

A series of second-generation compounds analogous to Santacruzamate A were designed, synthesized, and evaluated for their selective cytotoxic activity against the breast cancer cell line MDA-MB-231 (ATCC HTB-26). Compound 7 demonstrated the highest cytotoxicity and selectivity among the tested compounds, with an IC_{50} value of 8.30 μM, comparable to those of the positive controls cisplatin (8.46 μM) and etoposide (12 μM). *In silico* studies identified histone deacetylase 8 (HDAC8) as a potential target of compound 7, supporting its role as an HDAC inhibitor. Experimental data further confirmed the pro-apoptotic activity of compound 7, as it significantly increased caspase-3 and caspase-9 activities, along with TP53 and BAK expression compared to the untreated group. These findings indicate that compound 7 induces apoptotic cell death in tumor cells through the intrinsic mitochondrial pathway. This study highlights compound 7 as a promising candidate for further exploration as a selective anticancer agent targeting breast cancer cells.

Keywords: Synthesis. Santacruzamate A analogs. HDACi. Apoptosis. Cytotoxic activity.

***Correspondence**: T. R. Freitas, Núcleo de Pesquisa em Química Biológica (NQBio), Universidade Federal de São João del-Rei, Campus Centro Oeste, Divinópolis, MG, Brasil, E-mail: tuliorfreitas@gmail.com, https://orcid.org/0000-0002-2289-2201; F. P. Varotti, Núcleo de Pesquisa em Química Biológica (NQBio), Universidade Federal de São João del-Rei - Campus Centro Oeste, Divinópolis, MG, Brasil, E-mail: varotti@ufsj.edu.br, https://orcid.org/0000-0002-2939-7780. F. F. Hilário, Departamento de Química (DEQUI), Instituto de Ciências Exatas e Biológicas (ICEB), Universidade Federal de Ouro Preto - Campus Universitário Morro do Cruzeiro, Ouro Preto, MG, Brasil, E-mail: flavianehilario@ufop.edu.br, https://orcid.org/0000-0002-9003-2801, S. F. de Andrade - https://orcid.org/0009-0002-7687-3097. F. C. G. Evangelista - https://orcid.org/0000-0003-4682-397X. S. N. Andrade - https://orcid.org/0000-0002-1975-0827. C. L. Duarte - https://orcid.org/0000-0001-8003-606X. H. B. dos Santos - https://orcid.org/0000-0001-6813-8522. R. G. Thomé - https://orcid.org/0000-0002-1779-5036. J. L. Humberto - https://orcid.org/0009-0001-9688-1812. R. P. de Freitas - https://orcid.org/0000-0001-6974-3724. A. P. Sabino - https://orcid.org/0000-0001-8562-8689

INTRODUCTION

Breast cancer is the second most common cancer in the world, and it ranks first among women in terms of volume and fifth in number that results in death from cancer (Sung *et al.*, 2021; World Health Organization, 2020). Chemotherapy remains one of the main breast cancer treatment options (Bou Zerdan *et al.*, 2022; Obidiro, Battogtokh, Akala, 2023; Popolin *et al.*, 2017). Although most patients respond favorably to the initial application of chemotherapy, concerns related to its long-term efficacy and safety/tolerability toxicity/side effects remain (Chen *et al.*, 2018; Corrie, 2011). At the same time, breast cancer treatments are further facilitated by the disease relapse rate which increases due to chemoresistance in chemotherapy, and as a result

breast cancer treatment becomes more challenging (Chen *et al.*, 2018; Vidal *et al.*, 2014).

Triple-negative breast cancer (TNBC) represents about 15 to 20% of all breast cancer cases. TNBC is the most aggressive subtype because it does not express the receptors associated with hormonal signaling (estrogen and progesterone) or amplification of the HER2 receptor which would target TNBC for hormonal therapy, and therapies against HER2 such as Herceptin(Bianchini *et al.*, 2022; Obidiro, Battogtokh, Akala, 2023; Yin *et al.*, 2020). Therefore, the care standard for TNBC has continued to be chemotherapy. Nonetheless, TNBCs are often resistant to chemotherapy and patients have a high risk of relapse, chemoresistance, and ending with a poor clinical outcome (Bianchini *et al.*, 2022). These complications accentuate the pressing necessity for novel therapies.

Histone deacetylase (HDAC) inhibitors (HDACi) have emerged as a potential alternative to traditional treatments (Ramaiah *et al.*, 2021). Studies have shown that HDACi can modify the acetylation status of histone and non-histone proteins, thereby regulating cellular processes such as differentiation, survival, and apoptosis in cancer cells (von Knethen, Brüne, 2019; Mehmood *et al.*, 2023; Shanmugam, Rakshit, Sarkar, 2022).

HDACs are enzymes that remove acetyl groups from lysine residues, leading to chromatin condensation and transcriptional repression (Chen *et al.*, 2008; Guadagni *et al.*, 2024; Manal *et al.*, 2016; Ramaiah *et al.*, 2021). By inhibiting this process, HDACi influence gene expression involved in differentiation, apoptosis, angiogenesis, and inflammation, while also affecting non-histone proteins to regulate processes like cell cycle arrest (Mottamal *et al.*, 2015; Schizas *et al.*, 2018).

One key mechanism by which HDACi impact the cell cycle is through upregulation of the p21 gene, which plays a critical role in signaling the transition from the G1 phase to the S phase (Chen *et al.*, 2008; Schizas *et al.*, 2018). However, HDACi also affect multiple pathways, and their limited enzymatic specificity presents challenges for rational drug design tailored to specific diseases. Despite this complexity, various classes of HDACi have shown potent anticancer activity with notable tumor specificity in clinical studies, underscoring their diverse mechanisms of action (Guadagni *et al.*, 2024; Mottamal *et al.*, 2015; Shanmugam, Rakshit, Sarkar, 2022).

To date, four HDACi have been approved for cancer therapy by the U.S. Food and Drug Administration (FDA). Among them, Verinostat, Belinostat, and Panobinostat belong to the hydroxamate class and are described as having broad inhibition activity against various HDAC types (Chen *et al.*, 2008; Richon, 2006; Schizas *et al.*, 2018). However, this general lack of selectivity is believed to contribute to many of the undesirable side effects of these drugs, driving an increased search in recent years for more selective HDACi, particularly targeting cancer-related isoforms. In contrast to hydroxamates, Romidepsin, the only other HDAC inhibitor on the market, exhibits selectivity for class I HDAC isoforms. However, this selectivity does not extend within this class, as it remains active against HDACs 1, 2, 3, and 8 (Pavlik *et al.*, 2013).

In the last decade, Pavlik *et al.* (2013) reported isolation and elucidation of the structure and activity of a new inhibitor of HDACs, Santacruzamate A (SCA). SCA is a single isolated molecule from a marine cyanobacterium and embodies the classic pharmacophoric models for HDAC inhibition, featuring an ethyl carbamate terminus, a modified γ-aminobutyric acid (GABA) linker, and a phenethylamine cap group (Pavlik *et al.*, 2013).

Despite sharing a chemical structure akin to Verinostat, an FDA-approved drug for use in patients with Cutaneous T-Cell Lymphoma (CTCL) in October 2006, studies demonstrate that SCA selectively inhibits HDAC2, 4, and 6 at peak concentrations of micromolar, nanomolar, and sub-nanomolar, respectively, which piqued our interest regarding this molecule's activity (Gromek *et al.*, 2016; Lin *et al.*, 2019; Randino *et al.*, 2017).

Thus, we systematically explored the three chemical regions of its structure to re-evaluate the previously reported cytotoxicity of SCA, modifying the

zinc-binding group, cap terminus, and linker region. This effort yielded seven derivatives, detailed in another study (Andrade *et al.*, 2018) as the first-generation, along with an additional four compounds referred to as the second-generation, all of which underwent evaluation of their cytotoxic and immunomodulatory activities in this investigation.

MATERIAL AND METHODS

Material and compounds synthesis

All reagents were purchased from commercial suppliers. Solvents were purified or dried using conventional methods before use. Reactions were monitored by thin-layer chromatography (TLC, silica gel 60), utilizing iodine or ultraviolet light (254 nm) for visualization. Flash column chromatography was conducted on silica gel 0.04–0.063 mm (230–400 mesh). IR spectra were collected on an AAB Bomen MB3000 FTIR spectrometer (400-4000 cm^{-1}). NMR spectroscopy was performed on a Bruker Advance DRX at 200 or 400 MHz for ^{1}H-NMR and 50.32 or 100.64 MHz for^{13}C-NMR. Chemical shifts are reported in ppm (δ) relative to that of tetramethylsilane (TMS) as an internal standard or relative to the solvents' shifts: ^{1}H δ($CDCl_3$) = 7.26 ppm and ^{13}C δ($CDCl_3$) = 77.23 ppm, ^{1}H δ(CD_3OD) = 4.87 ppm and ^{13}C δ(CD_3OD) = 49.00 ppm. Accurate mass measurements (high-resolution mass spectrometry (HRMS)) were conducted using a Bruker Daltonics micrOTOF electrospray ionization mass spectrometer coupled with time-of-flight (Solvent: CH_3OH). Melting points were recorded on a Buchi B-540 apparatus and were left uncorrected.

Synthesis of ethyl (6-(4-hydroxybenzamido)hexyl carbamate (3)

4-Hydroxybenzoic acid (334 mg, 2.42 mmol) was added to *N*,*N*-dimethylformamide (10 mL) followed by the addition of ethyl (6-aminohexyl)carbamate (456 mg, 2.42 mmol). The solution obtained was cooled to 0°C and then 1-hydroxybenzotriazole (393 mg, 2.91 mmol), dicyclohexylcarbodiimide (600 mg, 2.91 mmol), and triethylamine (400 µL, 2.91 mmol) were added. The mixture was stirred at 0°C for 60 min and then 20-30°C for 24 h. The *N*,*N*-dimethylformamide was removed and the crude product was diluted in ethyl acetate (EtOAc, 30 mL). The obtained solution was washed with 10 % citric acid (w/v) (30 mL), 4% sodium bicarbonate (w/v) (25 mL), and brine (25 mL). The layer organic was dried over Na_2SO_4, filtered, and concentrated, resulting in crude product that was purified by silica gel chromatography (CH_2Cl_2:CH_3OH - 99:1, 98:2, 97.5:2.5) to afford compound **3** (537 mg, 1.74 mmol, 72%) as a white solid.

TLC (CH_2Cl_2:CH_3OH, 95:5) Rf = 0.76, mp: 75.1-75.9°C.

HRMS (ESI-TOF) m/z calcd for $C_{16}H_{25}N_2O_4^+$ [$(M+H)^+$] 309.1809, observed 309.1792.

^{1}H-NMR (400 MHz, CD_3OD), δ (ppm): 1.23 (t, *J* = 8.00 Hz, 3H), 1.36-1.44 (m, 4H), 1.48-1.55 (m, 2H), 1.59-1.64 (m, 2H), 3.10 (t, *J* = 8.00 Hz, 2H), 3.33-3.38 (m, 3H), 4.40-4.09 (m, 2H), 6.84 (d, *J* = 8.00 Hz, 2H) and 7.71 (d, *J* = 8.00 Hz, 2H).

^{13}C-NMR (100.64 MHz, CD_3OD), δ (ppm): 15.00, 27.47, 27.69, 30.50, 30.84, 40.81, 41.56, 61.57, 116.04, 126.67, 130.15, 159.22, 161.88 and 170.04.

IR ν_{max} (attenuated total reflection) 3389, 3293, 3100, 2939, 1696, 1632, 1605, 1537, 1503, 1346, 1264, 1149, 1043, 842 and 767 cm^{-1}.

Synthesis of ethyl (6-(4-(prop-2-yn-1-yloxy)benzamido) hexyl carbamate (5)

Potassium carbonate (253 mg, 1.83 mmol) was added to the compound **3** solution (246 mg, 0.80 mmol) in acetone (4 mL) The resulting suspension was cooled to 0°C and 2-propynyl methanesulfonate (133 mg, 0.99 mmol) dissolved in acetone (1 mL) was added dropwise. The mixture obtained was stirred at 60°C for 25 h. Then, distilled water (20 mL) was added to the reaction, which was then extracted with EtOAc (3 × 15 mL). The organic layer was dried over Na_2SO_4, filtered,

and concentrated, resulting in a crude product that was purified by silica gel chromatography (hexane:EtOAc - 6:4, 5:5) to afford compound **5** (160 mg, 0.46 mmol, 58%) as a white solid.

TLC (hexane:EtOAc, 3:7) Rf = 0.75, mp: 113.4-116.4°C.

HRMS (ESI-TOF) m/z calcd for $C_{19}H_{27}N_2O_4^+$ [$(M+H)^+$] 347.1965, observed 347.1980.

^{1}H-NMR (400 MHz, $CDCl_3$), δ (ppm): 1.23 (t, *J* = 8.00 Hz, 3H), 1.35-1.39 (m, 4H), 1.44-1.54 (m, 2H), 1.57-1.64 (m, 2H), 1.85-2.05 (sl, 1H), 2.54 (t, *J* = 4.00 Hz, 1H), 3.13-3.20 (m, 2H), 3.39-3.46 (m, 2H), 4.10 (q, *J* = 6.66 Hz, 2H), 4.73 (d, *J* = 4.00 Hz, 2H), 6.22-6.34 (sl, 1H), 7.00 (d, *J* = 8.00 Hz, 2H) and 7.76 (d, *J* = 8.00 Hz, 2H)

^{13}C-NMR (100.64 MHz, $CDCl_3$), δ (ppm): 14.86, 26.25, 26.47, 29.79, 30.16, 39.89, 40.81, 56.06, 60.94, 76.17, 78.19, 114.88, 128.15, 128.87, 157.06, 160.14 and 167.17.

IR ν_{max} (attenuated total reflection) 3398, 3287, 3257, 2927, 2125, 1700, 1641, 1600, 1541, 1509, 1271, 1221, 1179, 1020 and 844 cm^{-1}.

Synthesis of ethyl 6-(4-((1-(7-(diethylamino)-2-oxo-2H-chromen-3-yl)-1H-1,2,3-triazol-4-yl)methoxy) benzamido) hexyl carbamate (7)

Compound **5** (292 mg, 0.84 mmol) was added to ethanol (4 mL) in a reaction flask and covered with aluminum foil. Then, 3-azide-7-(diethylamino)-2*H*-chromen-2-ona (434 mg, 1.68 mmol), copper(II) sulfate pentahydrate (27 mg, 0.10 mmol) dissolved in distilled water (2 mL), and sodium ascorbate (53 mg, 0.26 mmol) dissolved in distilled water (2 mL) were added to the reaction flask. The mixture obtained was stirred at 20-30°C for 25 h. Distilled water (15 mL) was added to the reaction and it was extracted with dichloromethane (CH_2Cl_2, 4 × 15 mL). The organic layer was dried over Na_2SO_4, filtered, and concentrated, resulting in a crude product that was purified by silica gel chromatography (CH_2Cl_2:CH_3OH - 100:0, 99:1, 98:2) to afford compound **7** (332 mg, 0.31 mmol, 65%) as a green solid.

TLC (CH_2Cl_2:CH_3OH, 95:5) Rf = 0.77, mp = 192.5-195.3°C.

HRMS (ESI-TOF) m/z calcd for $C_{32}H_{41}N_6O_6^+$ [$(M+H)^+$] 605.3082, observed 605.3118.

^{1}H-NMR (400 MHz, $CDCl_3$), δ (ppm): 1.19-1.27 (m, 9H), 1.38-1.42 (m, 4H), 1.47-1.52 (m, 2H), 1.57-1.64 (m, 2H), 3.16-3.18 (m, 2H), 3.40-3.49 (m, 6H), 4.09 (q, *J* = 6.66 Hz, 2H), 4.72-4.78 (sl, 1H), 5.30-5.32 (m, 2H), 6.27-6.35 (sl, 1H), 6.58-6.61 (m, 1H), 6.72 (dd, *J* = 8.00 Hz, *J* = 4.00 Hz, 1H), 7.05 (d, *J* = 12.00 Hz, 2H), 7.43 (d, *J* = 8.00 Hz, 1H), 7.76 (d, *J* = 8.00 Hz, 2H), 8.40 (s, 1H) and 8.66 (s, 1H).

^{13}C-NMR (100.64 MHz, $CDCl_3$), δ (ppm): 12.56, 14.84, 26.23, 26.46, 29.76, 29.87, 30.11, 31.10, 39.82, 40.71, 45.35, 60.84, 62.03, 97.44, 107.39, 110.51, 114.77, 127.82, 128.92, 130.28, 135.06, 151.69, 156.00, 157.07, 160.84 and 167.22.

IR ν_{max} (attenuated total reflection) 3333, 3294, 2927, 1719, 1689, 1605, 1538, 1431, 1341, 1246, 1180, 1132, 1049, 999 and 818 cm^{-1}.

Synthesis of 6-(4-(prop-2-yn-1-yloxy)benzamido) hexanoic acid (6)

Compound **6** was synthetized from the basic hydrolysis of the methyl 6-(4-(prop-2-yn-1-yloxy) benzamido) hexanoate. The synthesis of this compound was described in the article about the Santacruzamate A first-generation analogs (Andrade *et al.*, 2018). First, LiOH (112 mg, 2.68 mmol) in water (5 mL) was added to a solution of methyl 6-(4-(prop-2-yn-1-yloxy) benzamido) hexanoate (250 mg, 0.82 mmol) in THF (5 mL). The mixture was stirred at room temperature for 24 h. A 5% aqueous solution of H_3PO_4 was added until pH 3, and the organic phase was extracted with EtOAc, dried over Na_2SO_4, filtered, and concentrated, resulting in a crude product that was purified by silica gel chromatography (CH_2Cl_2:CH_3OH - 100:0, 99:1, 98:2) to afford compound **6** (189 mg, 0.65 mmol, 79%) as a white solid.

TLC (hexane:EtOAc, 3:7) Rf = 0.1, mp = 134.0-135.5°C.

HRMS (ESI-TOF) m/z calcd for $C_{16}H_{18}NO_4^-$ [$(M-H)^-$] 288.1241, observed 288.1249.

^{1}H-NMR (200 MHz, CD_3OD), δ (ppm): 1.30-1.42 (m, 2H), 1.52-1.67 (m, 4H), 2.25 (t, *J* = 8.00 Hz, 2H), 2.91-2.94 (m, 1H), 3.23-3.33 (m, 2H), 4.73 (t, *J* = 4.00 Hz, 2H), 6.97 (d, *J* = 10.00 Hz, 1H), 7.73 (d, *J* = 8.00 Hz, 2H).
^{13}C-NMR (50.32 MHz, CD_3OD), δ (ppm): 25.77, 27.57, 30.22, 34.85, 40.79, 56.71, 77.13, 79.32, 115.68, 128.70, 129.98, 161.70, 167.50 and 177.58.
IR ν_{max} (attenuated total reflection) 3369, 3242, 3135, 2939, 2123, 1750, 1637, 1500, 1360, 1239, 1190, 1115, 1032, 824 and 760 cm^{-1}.

Cell culture

MDA-MB-231 human breast adenocarcinoma cell line (ATCC® HTB-26TM) and the WI-26VA4 human lung fibroblast line (ATCC® CCL-95.1TM) were grown in RPMI-1640 medium supplemented with 10% fetal bovine serum (FBS) and gentamicin (100 µg/mL). Cultures were maintained at 37°C in a humidified atmosphere with 5% CO_2.

Assessment of cell viability by MTT assay

Cell viability was assessed through the MTT (3-[4,5-dimethylthiazol-2-yl]-2,5-diphenyl-tetrazolium bromide) assay. First, 100 µL of complete medium containing 1×10^4 cells (MDA-MB-231 or WI-26VA4 cells) was added to each well of a 96-well tissue culture microtiter plate. Incubation occurred at 37°C in a humidified 5% CO_2 incubator for 24 hours prior to experimentation. Post medium removal, 100 µL of fresh medium, along with test compounds at concentrations ranging from 0.01 to 100 µg/mL, was added to each well and incubated at 37°C for 48 hours. All test compounds were pre-solubilized in dimethyl sulfoxide (DMSO) to prepare a stock solution of 10,000 µg/mL. It is important to note that the final DMSO concentration used in the treatment was strictly controlled at all of the experiment stages (≤ 0.2%), ensuring that its effect did not interfere with the results obtained. The medium was subsequently replaced with 100 µL of MTT solution (0.5 mg/mL) per well, followed by an additional 3 hour incubation under previous conditions. Next, 100 µL of DMSO was introduced into each well to dissolve formazan crystals. Absorbance (Abs) at 550 nm was measured using a microplate reader (Spectramax M5e, Molecular Devices, Sunnyvale, CA, USA). The growth inhibition percentage was calculated using the formula [1-(Abs of treated/Abs of control)]×100. All experiments were performed in triplicate, and results were expressed as mean IC_{50} values. IC_{50} values were calculated using OriginPro 8.0 software (OriginLab Corporation, Northampton, MA, USA). Selectivity index (SI) was computed based on IC_{50} values for each compound, with the formula: $SI = IC_{50}\ Y / IC_{50}\ X$

In which: IC_{50} X represents the IC_{50} value for MDA-MB-231 cell lines, and IC_{50} Y represents the IC_{50} value for WI-26VA4, the human non-tumor cell line.

Inverse virtual screening

The molecular targets chosen for molecular docking were obtained from Our Own Molecular Targets (OOMT) (Carregal *et al.*, 2017), which consists of validated targets sourced from the Protein Data Bank (PDB) (Berman *et al.*, 2013). The targets and their corresponding PDB codes used were: 3MAX (HDAC2), 4A69 (HDAC3), 3ZNR (HDAC7), 1W22 (HDAC8), and 1XQH (methyltransferase). Each molecular target's protonation state was adjusted to simulate a physiological pH of 7.4. All compounds were simultaneously constructed using the MarvinSketch program, ensuring their protonation states were appropriate for pH 7.4. The ligands subsequently underwent refinement using the MOPAC program with the PM7 semi-empirical method (Stewart, 2016). Next, each compound was docked to its respective molecular target using Autodock Vina software in conjunction with Octopus software (Maia *et al.*, 2017; Trott, Olson, 2010). Following docking, the pharmacophore map of the best target was generated using Discovery Studio Visualizer 4.0 (Accelrys Software, Inc., San Diego, CA, United States). This process facilitated identifying the optimal compound for the molecular targets under study.

Annexin V/PI staining assay for apoptosis

Cells were assessed for apoptosis via flow cytometry using the Annexin V-FITC Apoptosis Detection kit (BD Biosciences, cat # 556547, USA) in strict accordance with the manufacturer's instructions. MDA-MB-231 cells were treated with compound 7 (8.30 µM) for 48 hours, using a concentration of 1×10^6 cells per well in a 6-well tissue culture plate. Following treatment, cells were washed twice with phosphate-buffered saline (PBS) and then suspended in 0.15 mL of 1x annexin binding buffer. The cells were then labeled with 50 µL of the labeling mix containing 2.5 µL of annexin V-fluorescein isothiocyanate (FITC) and 2.5 µL of propidium iodide (PI) (3 mM), followed by a 15-minute incubation at 4°C in the dark. A flow cytometer (LSRFortessa™, BD Biosciences) was employed to quantify cells, analyzing 20,000 events. Non-stained controls were utilized to assess cell autofluorescence, while untreated cell controls were labeled with annexin V and PI to evaluate cell death in untreated cells. The population of cells in each quadrant was determined using FlowJo x 10.0.7 software.

Caspase-3 and -9 colorimetric assays

The enzymatic activities of caspase-3 and -9 were evaluated using colorimetric assays obtained from R&D Systems (Wiesbaden-Nordenstadt, Germany). Approximately 1×10^6 MDA-MB-231 cells were seeded in a 12-well tissue culture plate and incubated at 37°C in a humidified 5% COÁ incubator. After 24 hours, the medium was replaced, and the cells were treated with compounds at their respective IC_{50} values for 48 hours. Following treatment, cells were harvested, centrifuged, and washed twice with PBS. Cell samples were then sonicated in cell lysis buffer supplemented with protease inhibitors. The homogenates were centrifuged at 20,000 x g for 30 minutes, and the resulting supernatant was incubated with caspase-3 and -9 substrates (DEVD-pNA) at 37°C for 2 hours. The absorbance of each sample was measured at 405 nm, and the activity of caspase-3 and -9 was determined by the color reaction, which was directly proportional to their enzymatic activity.

p21 (CDKN1A), TP53, BAK and BCL-2 gene expression

Total RNA extraction was performed using Trizol LS reagent (Invitrogen Corporation 10296-010, Carlsbad, CA, USA) in strict accordance with the manufacturer's recommendations. Only compounds demonstrating satisfactory cytotoxic effects were further investigated. RNA extraction was performed from cells both before drug exposure and 48-hours post-treatment, with tested concentrations of each compound corresponding to the IC_{50}. The total RNA obtained after extraction was quantified using spectrophotometry (NanoVue, GE Healthcare Life Sciences, UK). Samples utilized in the study exhibited concentrations exceeding 50 ng/µL and purities between 1.7 and 1.9. The extracted RNAs underwent reverse transcriptase reactions to generate cDNAs, employing the High-Capacity cDNA Reverse Transcription Kit® (Applied Biosystems, USA). mRNA expression analysis of *p21 (CDKN1A)*, *TP53*, *BAK*, and *Bcl-2* was conducted via real-time PCR utilizing SYBR® Green methodology (Applied Biosystems) following supplier recommendations. PCR was performed on the StepOne Real-Time PCR System (Applied Biosystems) under the following conditions: 2 minutes at 50°C, 10 minutes at 95°C, followed by 40 cycles of 95°C for 15 seconds and 60°C for 1 minute. Quantification of each sample was conducted in triplicate using the ΔΔCT method, with all transcripts normalized to the endogenous GAPDH control. All reactions were subjected to uniform analysis conditions and normalized using the ROX passive reference dye signal to correct for fluctuations in reading resulting from volume changes and evaporation during PCR cycling.

Statistical analysis

The presented values include means accompanied by their corresponding standard deviations (SD). IC_{50} values were determined using OriginPro 8.0 software (OriginLab Corporation, Northampton, MA, USA). Comparison of data between control and test groups was performed using Student's t-tests. Gene expression outcomes were evaluated using Sigma Stat version 2.03 software. Each recorded value represents the average of no fewer than three independent experiments conducted within each group. Analysis of variance (ANOVA) was applied, followed by Tukey's multiple comparison test for normally distributed data. The non-parametric Kruskal-Wallis test was employed, followed by the Holm-Sidak multiple comparison test in cases where data deviated from a normal distribution. Significantly different values from the control are denoted by asterisks ($*p \leq 0.05$).

RESULTS AND DISCUSSION

Synthesis

The classic pharmacophore for zinc-dependent HDAC (a metalloenzyme) inhibition is formed by three distinct groups: 1) a zinc-binding group (ZBG); 2) a lipophilic cell recognition group; and 3) a hydrophobic linker of about 7.8 Å length (about five carbon atoms) that connects groups 1) and 2) (Chen *et al.*, 2008; Fierz, Muir, 2014; Pavlik *et al.*, 2013; Traoré *et al.*, 2013). Carbonyl groups like ketone, α-hydroxy-ketone, hydroxamate, ester, carbamate, thioester, or carboxylate groups are found to be a privileged ZBG in many natural or synthetic zinc-dependent HDAC inhibitor compounds. These different ZBGs have different capacities for zinc chelation, thus modification of ZBG can modify the efficiency (IC_{50}) and selectivity of the zinc dependent HDAC inhibitor compounds (Day, Cohen, 2013; Traoré *et al.*, 2013).

The first-generation analogs of SCA that we synthesized contain the three structural motifs of the classic pharmacophore for zinc-dependent HDAC inhibition: a tert-butyl carbamate or a methyl ester, like ZBG; a 4-hydroxybenzamide or a 4-(prop-2-yn-1-yloxy)benzamide or a 4-((1-(7-(diethylamino)-2-oxo-2H-chromen-3-yl)-1H-1,2,3-triazol-4-yl)methoxy) benzamide), like the lipophilic cell recognition group; and a chain of five, six, or seven carbon atoms, like the linker region. Like ZBG, the second generation of new SCA analogs has an ethyl carbamate (like SCA (Pavlik *et al.*, 2013)) or a carboxylic acid (like GABA (Chen *et al.*, 2008)) group. In addition, we maintained the lipophilic cell recognition group (a 4-(prop-2-yn-1-yloxy) benzamide or a 4-((1-(7-(diethylamino)-2-oxo-2H-chromen-3-yl)-1H-1,2,3-triazol-4-yl) methoxy) benzamide), and linker region (a chain of five or six carbon atoms) like in the first generation SCA analogs. The synthesis of this second generation had the objective of verifying if the different ZBGs (ethyl carbamate or carboxylic acid groups) promoted modification in the efficiency (IC_{50}) and selectivity of the zinc dependent HDAC inhibition in relation to the first-generation compounds.

The synthetic route for the new second-generation SCA analogs is outlined in Figure 1, which is similar to the synthetic route for the first-generation SCA analogs (Andrade *et al.*, 2018). In the first step, the carboxylic acid 1 was coupled with methyl 6-aminohexanoate and ethyl(6-aminohexyl) carbamate under classical coupling conditions to obtain the amides 2 and 3, respectively. These compounds were treated with potassium carbonate to obtain the corresponding phenolates, which after reaction with 2-propynyl methanesulfonate furnished the ether alkynes 4 and 5. The 3-azide-7-(diethylamino)-2H-chromen-2-one was synthesized in three steps from ethyl nitroacetate using a Knoevenagel condensation as the key step. A copper (II)-catalyzed click reaction was employed for the synthesis of compound **7**, involving the terminal alkyne of ether 5 and the 3-azide-7-(diethylamino)-2H-chromen-2-one. The ester group of the compound 4 was converted to a carboxylic acid group by basic hydrolysis of the ester group, furnishing the compound 6 (Traoré *et al.*, 2013).

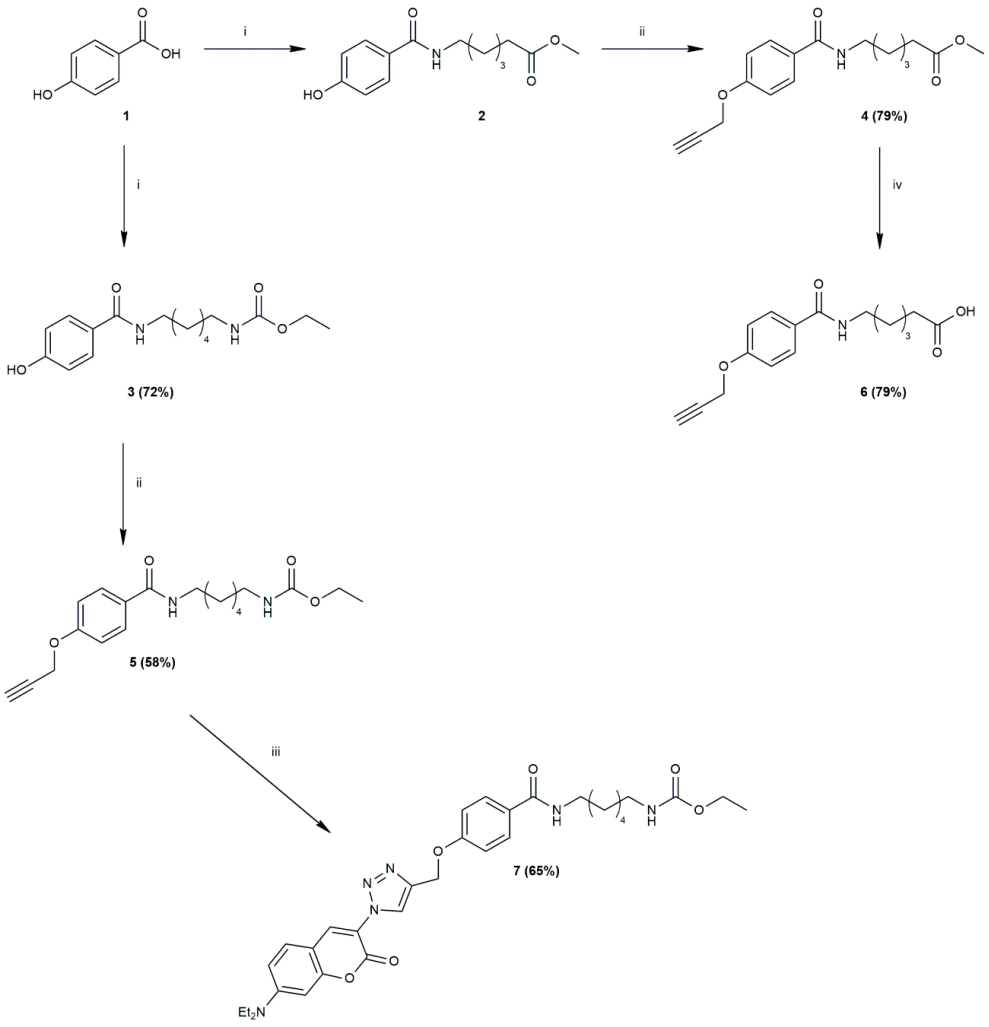

FIGURE 1 - Synthesis of new second-generation SCA analogs. Conditions: i) amine [methyl 6-aminohexanoate or ethyl(6-aminohexyl) carbamate], DMF, HOBt, DCC, Et_3N, 0°C (1 h) after 20-30°C (18-24 h); ii) K_2CO_3, 2-propynyl methanesulfonate, acetone, 60°C (25 h); iii) 3-azide-7-(diethylamino)-2H-chromen-2-ona, $CuSO_4 \cdot 5H_2O$, sodium ascorbate, ethanol:water (1:1), 20-30°C (25 h); iv) LiOH, THF:H_2O (1:1), 20-30°C (24 h).

All the new HDAC inhibitors were obtained in good yield and were evaluated for their anticancer activity.

Cytotoxicity assay

MTT assays were conducted on human MDA-MB-231 and WI-26VA4 (non-tumor cell line) cell lines to evaluate the cytotoxic efficacy of the compounds, with cisplatin, etoposide, and doxorubicin serving as reference cytotoxic agents. The resulting IC_{50} values are presented in Table I. The positive control groups were subjected to treatment with established cisplatin, etoposide, and doxorubicin chemotherapeutic agents, which have already gained clinical approval for combating ovarian cancer, leukemias, and breast cancer (Al-Oudat *et al.*, 2019; Bukowski, Kciuk, Kontek, 2020). Conversely, the negative control (viability control) remained untreated.

Thus, compound **7** exhibited higher potency and selectivity against the MDA-MB-231 tumor cell line

among the four tested compounds, displaying an IC_{50} value of 8.30 μM. Furthermore, it demonstrated a superior selectivity index in comparison to positive controls, which encompass established cancer treatment drugs. Prior investigations by our research group have corroborated this cytotoxic impact across seven additional first-generation Santacruzamate A analogs, specifically in breast and ovarian cancer cell lines (Andrade *et al.*, 2018).

The high cytotoxicity of compound **7** can be attributed to the presence of an aminocoumarin group linked through the triazolic ring in its structure. It is noteworthy that natural compounds derived from coumarin (a class of phenolic compounds characterized by an aromatic 1,2-benzopyrone ring and a benzene fused to the α-pyrone ring) have been reported to possess the ability to treat various types of cancer. The fusion of heterocyclic systems with the coumarin nucleus has emerged as a promising alternative for breast cancer treatment (Kaur *et al.*, 2015; Sandhu *et al.*, 2014).

Molecular modeling approach

Cancer development is known to involve epigenetic changes, including DNA methylation and histone acetylation modifications, which regulate accessibility of genetic material (Mottamal *et al.*, 2015). Recent studies have highlighted the interaction between histone methyltransferases (HMTs) and histone deacetylases (HDACs), which constitute crucial enzymes in these processes (Venkatesh, Workman, 2015).

In light of this, the potential target of compound **7** was identified through Inverse Virtual Screening. Compound **7** was docked into Our Own Molecular Targets, a database containing validated targets optimized for molecular docking calculations. Table II presents the binding energy values for various HDACs and methyltransferase, comparing them with the energies of the respective crystallographic compounds of each protein. All calculations were performed in triplicate.

The binding energies between the ligands and each HDAC ranged from -5.2 to -8.8 kcal/mol. Among these targets, compound **7** exhibited greater affinity against HDAC8 compared to the crystallographic compounds. Consequently, the interaction profile of compound **7** with HDAC8 was analyzed (Figure 2). Compound **7** formed a series of non-polar bonds with Cys275, Pro273, Asn307, Met274, Phe152, Phe207, and Tyr306 residues, and also formed hydrogen bonds with His180 and Leu308 residues. Despite these bonds contributing to the energy reduction, the compound did not interact with the zinc residue present in the protein site. This suggests the need for more robust

TABLE I - *In vitro* IC_{50} values obtained against MDA-MB-231 and WI-26VA4 cell lines

Compounds	IC_{50} (uM)[a]		Selective Index (SI)
	MDA-MB-231	WI-26VA4	MDA-MB-231
3	27.68 ± 22.24	$IC_{50} \geq 100$	≥ 3.61
5	$IC_{50} \geq 100$	$IC_{50} \geq 100$	≥ 1.00
6	$IC_{50} \geq 100$	98.65 ± 33.37	≤ 0.98
7	8.30 ± 2.65	69.30 ± 3.54	8.34
Cisplatin[b]	8.46 ± 1.41	1.35 ± 0.91	0.16
Etoposide[b]	12.00±1.07	8.65±0.23	0.72
Doxorubicin[b]	2.30±0.55	1.90±0.9	0.83

[a] IC_{50} values are shown as means ± SD of three independent experiments.; [b] Cisplatin, Etoposide and Doxorubicin used as positive controls.

TABLE II - Molecular docking of the compound **7** against HDACs and HMTs

Compound	ΔG Energy (kcal.mol-1)				
	HDAC2	**HDAC3**	**HDAC7**	**HDAC8**	**methyltransferase**
7	-8.7	-5.2	-8.8	-6.0	-7.8
Crystallographic Ligand	-9.9	-6.3	-10.4	-4.3	-8.0

calculations, such as molecular dynamics (Hospital *et al.*, 2015), to determine whether the compound will remain stable in the site or interact with the zinc atom upon binding to the protein.

Detection of apoptosis

The noteworthy reduction in the number of MDA-MB-231 cells observed in the cytotoxicity assay in the presence of compound **7** can be attributed to the potential activation of cell death mechanisms upon exposure to the compound. Indeed, numerous studies have already demonstrated the involvement of HDACis in various cellular processes, including apoptosis induction, reactive oxygen species generation, angiogenesis inhibition, and autophagy promotion (Ong *et al.*, 2012), shedding light on the action mechanism of HDACis.

Apoptosis is a tightly regulated process characterized by a series of biochemical events and structural changes, such as caspase activation, phosphatidylserine externalization, membrane blebbing, and nuclear fragmentation (Mollazadeh, Afshari, Hosseinzadeh, 2017). Understanding the fundamental mechanisms of apoptosis presents opportunities to identify novel therapeutic targets for diseases marked by an imbalance between cell proliferation and death, like cancer. At the outset of apoptosis, phosphatidylserine is translocated to the outer surface of the plasma membrane, detectable through the binding of fluorophore-labeled annexin V protein (Koopman *et al.*, 1994; Zhang, Chen, Liang, 2010).

Next, a flow cytometry analysis was conducted to explore the possibility that compound **7** was indeed inducing apoptotic cell death following 48 hours of treatment at the IC_{50} value. The assessment of cell death percentages through apoptosis and necrosis in MDA-MB-231 cells was performed after 48 hours of treatment with compound **7** (8.30 μM), followed by flow cytometric analysis. The graphs presented in Figure 3 depict the percentage of necrotic cells (Q1), cells in late apoptosis (Q2), cells in early apoptosis (Q3), and viable cells (Q4) after a 48-hour period in the presence of compound **7**. It is evident that there was a reduction of 95.45% in viable cells after treatment, along with an increase of 2.51% in cells in early apoptosis and a significant increase of 92.8% in cells in late apoptosis compared to the control group.

Zhou *et al.* (2018) also demonstrated the ability of five HDACis, including Santacruzamate A, to significantly induce apoptosis in tumor cells through flow cytometry, aligning with the results found in this study (Andrade *et al.*, 2018).

Studies have not yet suggested a detailed mechanism of action regarding the anticancer activity of coumarin derivatives. However, coumarin derivatives have been reported to induce apoptosis by negatively regulating the Bcl-2 protein and activating caspase-9, subsequently leading to activation of caspases-3, -6, and -7 in tumor cells of breast cancer, prostate cancer, and neuroblastomas (Kaur *et al.*, 2015).

Detection of caspase activation

Sequential activation of caspases assumes a pivotal role in the execution phase of cellular apoptosis

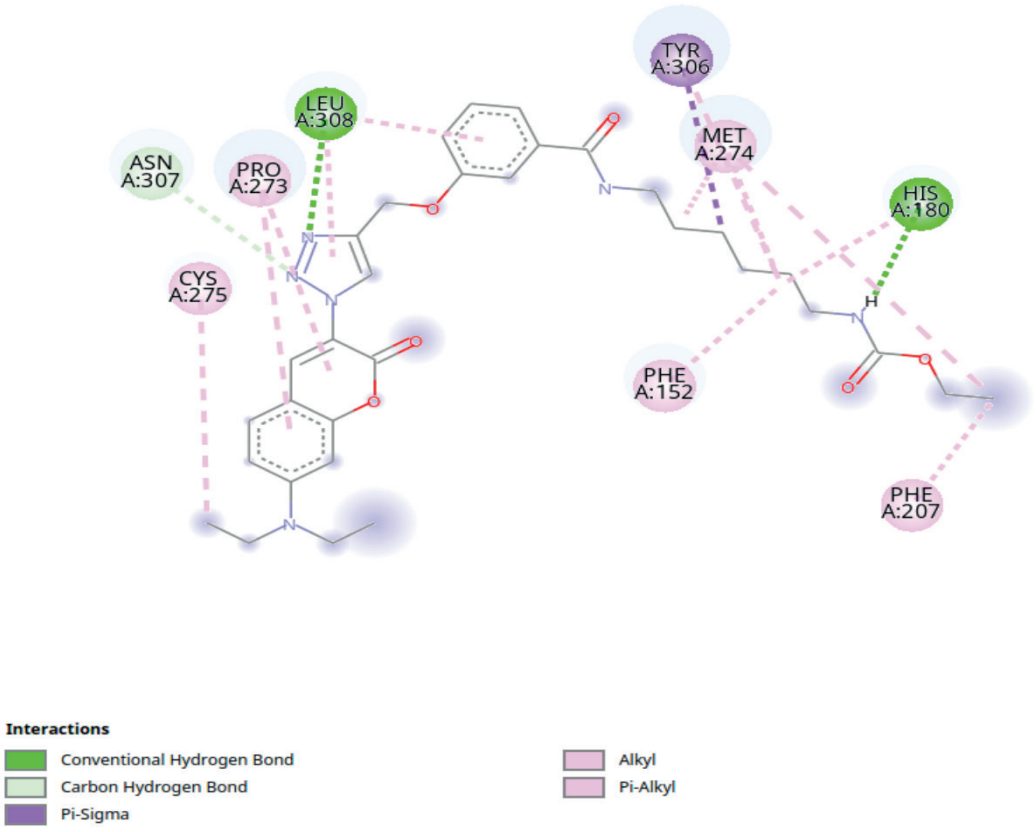

FIGURE 2 - Pharmacophoric map of compound 7 against HDAC8.

(McIlwain, Berger, Mak, 2013). Consequently, the activity of both caspase-3 and caspase-9 exhibited a notable increase, as clearly demonstrated in Figure 4. The zenith of enzymatic activity was discernible at the 48-hour mark post-exposure.

Upon a 48-hour incubation period, caspase 3 and caspase 9 activity displayed a substantial increase within the treated group (compound **7**) compared to the negative control group (untreated tumor cell line). Remarkably, the elevation in caspase 9 levels after treatment with compound **7** closely paralleled that of the positive control (cisplatin), indicating the initiation of apoptosis via the mitochondrial pathway (Li *et al.*, 2017). These findings align with numerous studies reporting that HDAC inhibitors render tumor cells more susceptible to apoptosis due to their ability to induce histone acetylation and provoke alterations in gene expression (Zhang, Zhong, 2014).

Analysis of *p21, TP53, BAK* and *BCL-2* gene expression

In order to understand the mechanism by which compound 7 was inducing cell death, we performed RT-qPCR on regulatory genes important in cell responses: *p21 (CDKN1A)*, *TP53*, *BAK* and *BCL-2*. The results, analyzed by ΔΔCT method, are shown in Figure 5. Incubation of MDA-MB-231 cells with compound 7 at its IC_{50} value (8.308 μM) for 4 8 h caused significant up-regulation of *TP53* and *BAK* and down-regulation of *BCL-2* compared with the untreated control group.

The p53 protein controls the phosphorylation of cyclin-dependent kinases (CDKs) and therefore regulates cell cycle progression, usually resulting in a

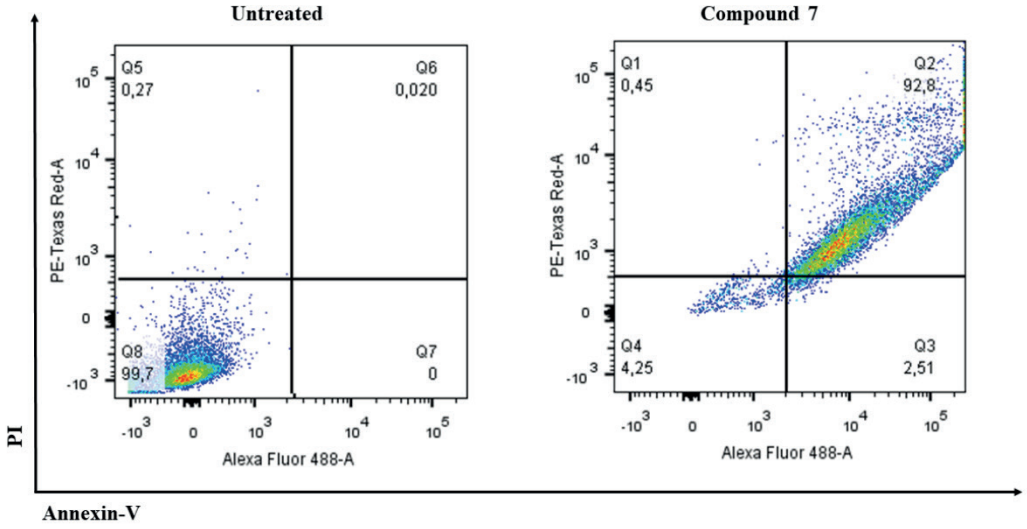

FIGURE 3 - Effect of compound **7** on apoptosis of MDA-MB-231 cells after 48 h of exposure. Apoptotic cells were analyzed by flow cytometry, and the scatter plot displays Annexin V fluorescence (x-axis, logarithmic scale) versus PI fluorescence (y-axis, logarithmic scale).

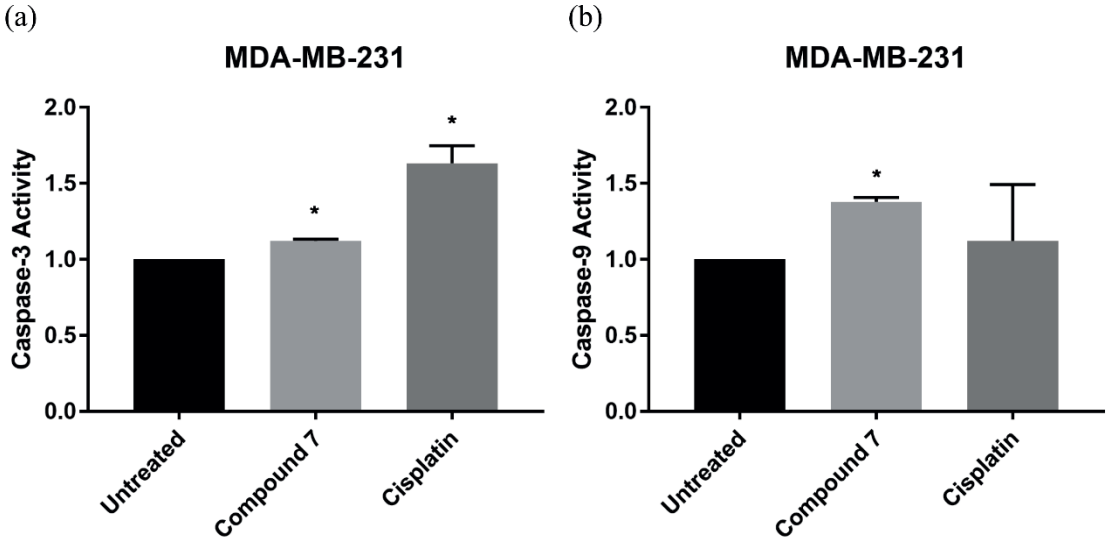

FIGURE 4 - Relative quantification of caspase-3 (a) and caspase-9 (b) activity by colorimetric assay in MDA-MB-231 cell line after 48 h of exposure to compound 7 (*$p<0.05$).

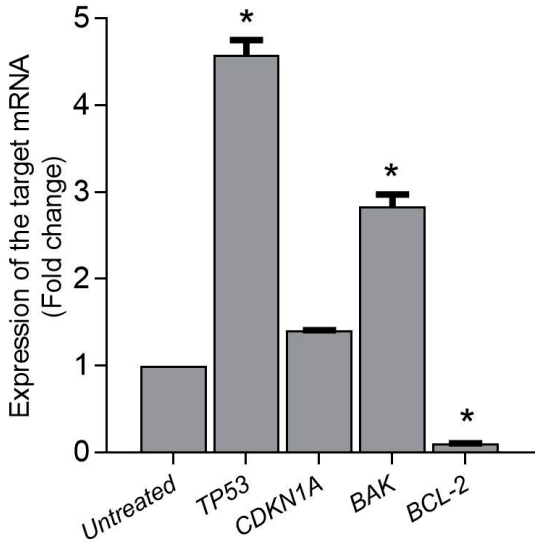

FIGURE 5 - Relative quantification of *TP53*, *CDKN1A*, *BAK*, and *BCL-2* mRNA levels in MDA-MB-231 cells after 48 h of exposure to compound 7 at its IC_{50} concentration (8.308 μM) (*p<0.05).

cell cycle arrest due to the transcriptional activation by p21 (Zhou *et al.*, 2018). For example, p21 is one of the main effectors of DNA repair or cell cycle regulation acting to arrest cells at G1/S checkpoint (Otto, Sicinski, 2017). Although p21 serves as a downstream target of the tumor suppressor p53 in most stress and DNA damage responses, it is reported to play context-dependent roles for apoptosis induction. Placed in different contexts, p21 can enhance cell survival or facilitate apoptotic processes depending on local milieu and stimulus (Volkmann *et al.*, 2014).

Although TP53 upregulation in this case indicates induction of the apoptotic response, the lack of a shift in CDKN1A (p21) expression suggests that compound 7 induces apoptosis independently of triggering the cell cycle arrest pathways typically associated with p21. These findings imply that p21 modulation does not represent the primary molecular mechanism driving apoptosis. Instead, we observed upregulation of the pro-apoptotic protein BAK and downregulation of the anti-apoptotic protein BCL-2, both of which are consistent with activation of the intrinsic (mitochondrial) apoptotic pathway.

However, the pathway activated by compound 7 appears to bypass p21-related checkpoints, favoring direct apoptosis via the mitochondrial/caspase route. Therefore, the apoptotic response seems to be p21-independent, with TP53 promoting cell death by upregulating pro-apoptotic genes of the BCL-2 family and interacting with anti-apoptotic genes, facilitating apoptotic cell death. Further investigation would be required to confirm this hypothesis.

CONCLUSION

Second-generation Santacruzamate A analogs exhibited cytotoxic activity against the MDA-MB-231 breast adenocarcinoma cell line. Compound **7** demonstrated the highest potency and selectivity among the analogs, displaying a significantly lower IC_{50} value (8.308 μM) compared to the other compounds and a notably elevated selectivity index (8.34) when contrasted with the positive controls. The *in silico* study further revealed that compound **7** interacted effectively with the proposed molecular targets. Notably, it displayed the strongest interaction with HDAC8. Furthermore, compound **7** is able to induce apoptosis via the mitochondrial pathway in a p53-dependent manner was demonstrated through the Annexin V/PI assay, the colorimetric activation analysis of caspase-3 and -9, and gene expression experiments. Hence, our findings strongly suggest that compound **7**, as evaluated in this study, holds significant promise as a potential candidate for future breast cancer chemotherapy.

ACKNOWLEDGMENTS

The authors would like to acknowledge the financial support received from the following institutions: *Coordenação* de Aperfeiçoamento de Pessoal de Nível Superior (*CAPES*), *Fundação de Amparo* à Pesquisa do Estado de Minas Gerais (*FAPEMIG*) and *Conselho Nacional de Desenvolvimento Científico e Tecnológico* (*CNPq*).

AUTHORS' CONTRIBUTIONS

The manuscript was written through contributions of all authors. F.P.V. and T.R.F. performed the study concept and design. T.R.F. drafted the manuscript. T.R.F., F.C.G.E., S.N.A., C.L.D., and S.F.A. developed the methodology. T.R.F. and F.P.V. reviewed and edited the paper. T.R.F., F.P.V., A.P.S., R.G.T., H.B.S., F.F.H., R.P.F., and J.L.H. performed the data interpretation and statistical analysis. All authors read and approved the final paper.

REFERENCES

Al-Oudat BA, Alqudah MA, Audat SA, Al-Balas QA, El-Elimat T, Hassan MA, et al. Design, synthesis, and biologic evaluation of novel chrysin derivatives as cytotoxic agents and caspase-3/7 activators. Drug Des Devel Ther. 2019;13:423–33. https://doi.org/10.2147/dddt.s189476.

Andrade SN, Evangelista FCG, Seckler D, Marques DR, Freitas TR, Nunes RR, et al. Synthesis, cytotoxic activity, and mode of action of new Santacruzamate A analogs. Med Chem Res. 2018;27:2397–413. https://doi.org/10.1007/s00044-018-2244-3.

Berman HM, Kleywegt GJ, Nakamura H, Markley JL. The future of the protein data bank. Biopolymers. 2013;99:218–22. https://doi.org/10.1002/bip.22132.

Bianchini G, De Angelis C, Licata L, Gianni L. Treatment landscape of triple-negative breast cancer — expanded options, evolving needs. Nat Rev Clin Oncol. 2022;19:91–113. https://doi.org/10.1038/s41571-021-00565-2.

Bou Zerdan M, Ghorayeb T, Saliba F, Allam S, Bou Zerdan M, Yaghi M, et al. Triple negative breast cancer: Updates on classification and treatment in 2021. Cancers (Basel). 2022;14. https://doi.org/10.3390/cancers14051253.

Bukowski K, Kciuk M, Kontek R. Mechanisms of multidrug resistance in cancer chemotherapy. Int J Mol Sci. 2020;21.

Carregal AP, Maciel F V, Carregal JB, dos Reis Santos B, da Silva AM, Taranto AG. Docking-based virtual screening of Brazilian natural compounds using the OOMT as the pharmacological target database. J Mol Model. 2017;23. https://doi.org/10.1007/s00894-017-3253-8.

Chen C, Lu L, Yan S, Yi H, Yao H, Wu D, et al. Autophagy and Doxorubicin resistance in cancer. Anticancer Drugs 2018;29:1–9. https://doi.org/10.1097/CAD.0000000000000572.

Chen PC, Patil V, Guerrant W, Green P, Oyelere AK. Synthesis and structure – activity relationship of histone deacetylase (HDAC) inhibitors with triazole-linked cap group. Bioorg Med Chem. 2008;16:4839–53. https://doi.org/10.1016/j.bmc.2008.03.050.

Chen Y, Lopez-Sanchez M, Savoy DN, Billadeau DD, Dow GS, Kozikowski AP. A series of potent and selective, triazolylphenyl-based histone deacetylases inhibitors with activity against pancreatic cancer cells and Plasmodium falciparum. J Med Chem. 2008;51:3437–48. https://doi.org/10.1021/jm701606b.

Corrie PG. Cytotoxic chemotherapy: Clinical aspects. Medicine. 2011;39:717–22. https://doi.org/10.1016/j.mpmed.2011.09.012.

Day JA, Cohen SM. Investigating the selectivity of metalloenzyme inhibitors. J Med Chem. 2013;56(20):7997-8007. doi: 10.1021/jm401053m.

Fierz B, Muir TW. Chromatin as an expansive canvas for chemical biology. Nat Chem Biol. 2014;8:417–27. https://doi.org/10.1038/nchembio.938.

Gromek SM, deMayo JA, Maxwell AT, West AM, Pavlik CM, Zhao Z, et al. Synthesis and biological evaluation of santacruzamate A analogues for anti-proliferative and immunomodulatory activity. Bioorg Med Chem. 2016;24:5183–96. https://doi.org/10.1016/j.bmc.2016.08.040.

Guadagni A, Barone S, Alfano AI, Pelliccia S, Bello I, Panza E, et al. Tackling triple negative breast cancer with HDAC inhibitors: 6 is the isoform! Eur J Med Chem. 2024;279. https://doi.org/10.1016/j.ejmech.2024.116884.

Hospital A, Goñi JR, Orozco M, Gelpí JL. Molecular dynamics simulations: Advances and applications. Adv Appl Bioinform Chem. 2015;8:37–47. https://doi.org/10.2147/AABC.S70333.

Kaur M, Kohli S, Sandhu S, Bansal Y, Bansal G. Coumarin: A Promising Scaffold for Anticancer Agents. Anticancer Agents Med Chem. 2015;15:1032–48. https://doi.org/10.2174/1871520615666150101125503.

von Knethen A, Brüne B. Histone Deacetylation Inhibitors as Therapy Concept in Sepsis. Int J Mol Sci. 2019;20:346. https://doi.org/10.3390/ijms20020346.

Koopman BG, Reutelingsperger CPM, Kuijten GAM, Keehnen RMJ, Pals ST, van Oers MHJ. Annexin V for flow cytometric detection of phosphatidylserine expression on B cells Undergoing apoptosis. Blood. 1994;84(5):1415-20.

Li P, Zhou L, Zhao T, Liu X, Zhang P, Zheng X, et al. Caspase-9: structure, mechanisms and clinical application. Oncotarget. 2017;8:23996–4008. https://doi.org/10.18632/oncotarget.15098.

Lin CL, Tsai ML, Lin CY, Hsu KW, Hsieh WS, Chi WM, et al. HDAC1 and HDAC2 double knockout triggers cell apoptosis in advanced thyroid cancer. Int J Mol Sci. 2019;20. https://doi.org/10.3390/ijms20020454.

Maia EHB, Campos VA, dos Reis Santos B, Costa MS, Lima IG, Greco SJ, et al. Octopus: a platform for the virtual high-throughput screening of a pool of compounds against a set of molecular targets. J Mol Model. 2017;23. https://doi.org/10.1007/s00894-016-3184-9.

Manal M, Chandrasekar MJN, Gomathi Priya J, Nanjan MJ. Inhibitors of histone deacetylase as antitumor agents: A critical review. Bioorg Chem. 2016;67:18–42. https://doi.org/10.1016/j.bioorg.2016.05.005.

McIlwain DR, Berger T, Mak TW. Caspase functions in cell death and disease. Cold Spring Harb Perspect Biol. 2013;5:1–28. https://doi.org/10.1101/cshperspect.a008656.

Mehmood SA, Sahu KK, Sengupta S, Partap S, Karpoormath R, Kumar B, et al. Recent advancement of HDAC inhibitors against breast cancer. Med Oncol. 2023;40. https://doi.org/10.1007/s12032-023-02058-x.

Mollazadeh H, Afshari AR, Hosseinzadeh H. Review on the potential therapeutic roles of Nigella sativa in the treatment of patients with cancer: Involvement of apoptosis: - Black cumin and cancer. J Pharmacopuncture. 2017;20:158–72. https://doi.org/10.3831/KPI.2017.20.019.

Mottamal M, Zheng S, Huang TL, Wang G. Histone deacetylase inhibitors in clinical studies as templates for new anticancer agents. Molecules. 2015;20:3898–941. https://doi.org/10.3390/molecules20033898.

Obidiro O, Battogtokh G, Akala EO. Triple negative breast cancer treatment options and limitations: Future outlook. Pharmaceutics. 2023;15. https://doi.org/10.3390/pharmaceutics15071796.

Ong PS, Wang XQ, Lin HS, Chan SY, Ho PC. Synergistic effects of suberoylanilide hydroxamic acid combined with cisplatin causing cell cycle arrest independent apoptosis in platinum-resistant ovarian cancer cells. Int J Oncol. 2012;40:1705–13. https://doi.org/10.3892/ijo.2012.1354.

Otto T, Sicinski P. Cell cycle proteins as promising targets in cancer therapy. Nat Rev Cancer. 2017;17:93–115. https://doi.org/10.1038/nrc.2016.138.

Pavlik CM, Wong CYB, Ononye S, Lopez DD, Engene N, McPhail KL, et al. Santacruzamate A, a potent and selective histone deacetylase inhibitor from the panamanian marine cyanobacterium cf. symploca sp. J Nat Prod. 2013;76:2026–33. https://doi.org/10.1021/np400198r.

Popolin CP, Reis JPB, Becceneri AB, Graminha AE, Almeida MAP, Corrêa RS, et al. Cytotoxicity and anti-tumor effects of new ruthenium complexes on triple negative breast cancer cells. PLoS One. 2017;12:1–21. https://doi.org/10.1371/journal.pone.0183275.

Ramaiah MJ, Tangutur AD, Manyam RR. Epigenetic modulation and understanding of HDAC inhibitors in cancer therapy. Life Sci. 2021;277. https://doi.org/10.1016/j.lfs.2021.119504.

Randino R, Gazzerro P, Mazitschek R, Rodriquez M. Synthesis and biological evaluation of Santacruzamate-A based analogues. Bioorg Med Chem. 2017;25:6486–91. https://doi.org/10.1016/j.bmc.2017.10.026.

Richon VM. Cancer biology: mechanism of antitumour action of vorinostat (suberoylanilide hydroxamic acid), a novel histone deacetylase inhibitor. Br J Cancer. 2006;95(S1):S2–6. https://doi.org/10.1038/sj.bjc.6603463

Sandhu S, Bansal Y, Silakari O, Bansal G. Coumarin hybrids as novel therapeutic agents. Bioorg Med Chem. 2014;22:3806–14. https://doi.org/10.1016/j.bmc.2014.05.032.

Schizas D, Mastoraki A, Naar L, Spartalis E, Tsilimigras DI, Karachaliou G-S, et al. Concept of histone deacetylases in cancer: Reflections on esophageal carcinogenesis and treatment. World J Gastroenterol. 2018;24:4635–42. https://doi.org/10.3748/wjg.v24.i41.4635.

Shanmugam G, Rakshit S, Sarkar K. HDAC inhibitors: Targets for tumor therapy, immune modulation and lung diseases. Transl Oncol. 2022;16. https://doi.org/10.1016/j.tranon.2021.101312.

Stewart JJP. MOPAC2016TM 2016. http://openmopac.net/MOPAC2016.html.

Sung H, Ferlay J, Siegel RL, Laversanne M, Soerjomataram I, Jemal A, et al. Global Cancer Statistics 2020: GLOBOCAN Estimates of Incidence and Mortality Worldwide for 36 Cancers in 185 Countries. CA Cancer J Clin. 2021;71:209–49. https://doi.org/10.3322/caac.21660.

Traoré M, Mietton F, Maubon D, Peuchmaur M, Francisco Hilário F, Pereira De Freitas R, et al. Flexible synthesis and evaluation of diverse anti-apicomplexa cyclic peptides. J Org Chem. 2013;78:3655–75. https://doi.org/10.1021/jo4001492.

Trott O, Olson A. NIH Public Access. J Comput Chem. 2010;31:455–61. https://doi.org/10.1002/jcc.21334. AutoDock.

Venkatesh S, Workman JL. Histone exchange, chromatin structure and the regulation of transcription. Nat Rev Mol Cell Biol. 2015;16:178–89. https://doi.org/10.1038/nrm3941.

Vidal SJ, Rodriguez-Bravo V, Galsky M, Cordon-Cardo C, Domingo-Domenech J. Targeting cancer stem cells to suppress acquired chemotherapy resistance. Oncogene. 2014;33:4451–63. https://doi.org/10.1038/onc.2013.411.

Volkmann N, Marassi FM, Newmeyer DD, Hanein D. The rheostat in the membrane: BCL-2 family proteins and apoptosis. Cell Death Differ. 2014;21:206–15. https://doi.org/10.1038/cdd.2013.153.

World Health Organization (WHO). Global Health Estimates 2020: Deaths by Cause, Age, Sex, by Country and by Region, 2000-2019 2020. who.int/data/gho/data/themes/mortality-and-global-health-estimates/ghe-leading-causes-of-death (accessed January 16, 2023).

Yin L, Duan JJ, Bian XW, Yu SC. Triple-negative breast cancer molecular subtyping and treatment progress. Breast Cancer Res. 2020;22. https://doi.org/10.1186/s13058-020-01296-5.

Zhang J, Zhong Q. Histone deacetylase inhibitors and cell death. Cell Mol Life Sci. 2014;71:3885–901. https://doi.org/10.1007/s00018-014-1656-6.

Zhang P, Chen J, Liang Y. DNA binding, cytotoxicity, and apoptotic-inducing activity of ruthenium(II) polypyridyl complex. Acta Biochim Biophys Sin. 2010;42:440–9. https://doi.org/10.1093/abbs/gmq040. Advance.

Zhou H, Cai Y, Liu D, Li M, Sha Y, Zhang W, et al. Pharmacological or transcriptional inhibition of both HDAC1 and 2 leads to cell cycle blockage and apoptosis via p21 Waf1/Cip1 and p19 INK4d upregulation in hepatocellular carcinoma. Cell Prolif. 2018;51:e12447. https://doi.org/10.1111/cpr.12447

Received for publication on July 22nd, 2024
Accepted for publication on December 11th, 2024
Associated Editor: Lusania Maria Antunes